JOURNAL OF GEOPHYSICAL RESEARCH, VOL. ???, XXXX, DOI:10.1029/,

Type II Solar Radio Bursts : 2. Detailed comparison of theory with observations

D. S. Hillan,[1,2] Iver. H. Cairns,[1] P. A. Robinson[1]

[1]School of Physics, University of Sydney,

Sydney, New South Wales, Australia.

[2]Now at: CSIRO Earth Science and

Resource Engineering, Sydney, New South

Wales, Australia.

Abstract. In this paper, the second in a two paper series, we quantitatively compare a detailed theory for type II solar radio bursts with observations and extract the parameters of the associated shocks. We use the techniques and assessment parameters developed and demonstrated in the companion paper for artificial data sets and solar wind models. Here we investigate three relatively well-observed type II events with estimates of shock parameters from LASCO/SOHO observations of coronal mass ejections (CMEs) or other data. Using these parameters we obtain reasonable qualitative and semiquantitative agreement (25-40% correlations) between the theory and observed dynamic spectra. Then, using an iterative downhilll simplex method with two assessment parameters, we extract model shock parameters that increase the agreement between theory and observation in terms of relative flux levels, spectral intensifications and drift rates. The extracted parameters agree qualitatively and semiquantitatively with the parameters (speed, size and expansion index) estimated from CME observations for one of the studied events. The extracted parameters agree qualitatively with the remaining two events and yield new initial shock speeds. The agreement between this multi-process theory and observations is promising for these first quantitative comparisons performed here. Quantitatively, the bulk of the radio emission agrees to within 5 to 10 dB with observations, with the theory typically overpredicting the intensity of bright spots in the dynamic spectra. The methods and analyses presented here show potential for the remote infer-

ence of CME-driven shock parameters and the prediction of radio and space weather events.

1. Introduction

Type II solar radio bursts have been observed for over half a century [*Wild*, 1950a, b; *Wild et al.*, 1963; *Cane et al.*, 1982]. They contain one or more bands of emission drifting down slowly in frequency. Often a pair of bands is observed, differing in frequency by a factor close to two. The drifting type II radiation has long been identified with emission near the local plasma frequency f_p and near $2f_p$ excited by a shock moving out through the solar corona and solar wind [*Wild et al.*, 1963; *Cane et al.*, 1982; *Cane*, 1985; *Nelson and Melrose*, 1985; *Cairns*, 1986, 2011]. Coronal mass ejections (CMEs) can drive shocks ahead of them that persist into the interplanetary medium, while shocks formed by steepening of blast waves likely do not persist [*Cane et al.*, 1987; *Reiner et al.*, 1998]. The shock moves antisunwards in the direction of decreasing solar wind number density, producing radio emission at metric to kilometric wavelengths. The frequencies of the type II bands are observed to track the local plasma frequency f_p and $2f_p$ source regions upstream of the shock [*Lengyel-Frey et al.*, 1997; *Reiner et al.*, 1998; *Bale et al.*, 1999].

A detailed model for type II bursts has been developed in recent years [*Knock et al.*, 2001; *Cairns et al.*, 2003; *Knock et al.*, 2003a, b; *Knock and Cairns*, 2005; *Cairns and Knock*, 2006; *Florens et al.*, 2007; *Schmidt and Gopalswamy*, 2008; *Cairns*, 2011]. The dynamic spectrum of a type II event may be simulated by calculating the radio emission produced in the foreshocks of a rippled paraboloidal model shock. A two-dimensional model of the solar wind plasma, driven by spacecraft data observed at 1AU, was recently coupled with the type II theory to investigate the effect of more realistic solar wind structures on the predicted dynamic spectra [*Florens et al.*, 2007]. Using this model, some aspects of the predicted and observed dynamic spectra agree reasonably well for the 24 August 1998 type II event studied by *Bale et al.* [1999]. However, this analysis was not fully quantitative and lacked a comprehensive model of the observed satellite background to be incorporated into theoretical spectra for detailed comparisons between theory and observation. A recent model by *Hillan et al.* [2010] of the background observed by the WAVES instrument onboard the spacecraft Wind allows us to directly compare the predicted type II spectra with spacecraft observations and to quantitatively investigate the agreement between theory and observation.

This paper is the second in a two part series that tests the application of the recently developed theory to type II solar radio burst events and their associated CME-driven shocks. The companion paper, part 1 [*Hillan et al.*, 2012], focuses on developing performance metrics and testing extraction of shock parameters from iterative comparisons between "observed" and predicted artificial type II dynamic spectra created with various solar wind models. In the present paper, part 2, we present the first detailed quantitative comparisons of the type II theory with observations. Parameters controlling the evolution of the CME-driven shock are shown to affect agreement and can be constrained. Specifically, iterative comparisons between theory and observation allow the shock and CME parameters to be estimated. This has important consequences for space weather prediction since it offers the potential for the time-varying three-dimensional shock location and associated shock parameters (including shock speed and arrival time at Earth) to be estimated remotely and with greater than 6-hour lead time, by comparing iterated theoretical model results with spacecraft radio data. This will likely require automated identification of interplanetary type II bursts, as already done for coronal type II and III bursts [*Lobzin et al.*, 2008, 2010].

This paper aims to: (i) Combine the model of *Hillan et al.* [2010] for the instrumental and natural background signals observable at 1 AU with the Wind/WAVES instrument, the type II theory [*Knock et al.*, 2001; *Cairns and Knock*, 2006] and the solar wind model of *Florens et al.* [2007] into a comprehensive theory for type II bursts. (ii) Perform detailed comparisons of theory and observations using analyses based on cross-correlation and a normalised deviation parameter. (iii) Demonstrate reasonable qualitative and semi-quantitative agreement for three relatively well-observed type II events. (iv) Demonstrate the effect of varying shock parameters on the predicted dynamic spectra and their agreement with observation. (v) Constrain the shock (and CME) parameters, by maximising the agreement between the type II observations and model. (vi) Discuss issues with the theory and observations, and suggest possible future resolutions.

The paper is organised as follows. Section 2 summarizes the theoretical model for type II bursts and explains the two measures used to quantify the agreement between theory and observation, based on the companion paper [*Hillan et al.*, 2012]. Section 3 introduces the three type II events studied in the paper and describes the shock parameters obtained from CME and other non-radio observations. Section 4 uses these estimates of the shock parameters for the three events to simulate the dynamic spectra and then uses two measures to assess the agreement between observation and theory. Section 5 uses the iterative minimisation methods discussed to constrain the free shock parameters and demonstrate better agreement between theory and observation than for the nominal shock parameters. Section 6 discusses the results and shows that on average the theory overpredicts the observed radiation level by around 5 to 10 dB. The results are summarized in Section 7.

2. Summary of model and method

This section is based on *Hillan et al.* [2012], which reviews the current type II theory and discusses the parameter extraction method in detail. We summarize the main points below.

A two-dimensional model of the solar wind plasma and magnetic field is obtained using the approach of *Florens et al.* [2007]. This assumes the wind is constant over a solar rotation correponding to a specific radio event and maps the time of observation at 1 AU by the Wind spacecraft to the heliolongitude of a source on the Sun using the monthly average of the (assumed radial) solar wind velocity. Parker-like magnetic field solutions, conservation of electron number and wind speed, and power-law relations are used to map the magnetic field and plasma quantities from the observations at 1 AU in heliolatitude and heliocentric distance. Eleven-point boxcar averages of 1-hour averaged Wind or ACE spacecraft data are used.

A CME-driven shock is modeled as a paraboloid, and packed with ripples of size determined by the local spatially-varying decorrelation length $L(h)$ of the magnetic field [*Knock et al.*, 2003b; *Knock and Cairns*, 2005; *Neugebauer and Giacolone*, 2005]. The upstream solar wind parameters for each ripple are specified by the data-driven solar wind model at each time step given by the characteristic ripple lifetime $\tau_r = r_c/V_A$. Here $r_c(h)$ is the ripple's radius of curvature, given by

$$r_c(h) = 10^9 \left(\frac{r}{1\ \mathrm{AU}}\right)^{1.61} , \tag{1}$$

and V_A is the Alfven speed.

The time-varying heliocentric distance to the paraboloid's vertex is given by h. This paraboloid has a global radius of curvature R_c that evolves according to

$$R_c(h) = s\left(\frac{h}{1\mathrm{AU}}\right)^{d+1}, \tag{2}$$

where s is the radius of curvature at 1 AU, and d is the expansion index. The shock vertex has an initial radial speed v_i, starting at 1.1 solar radii ($R_\odot$), with constant linear deceleration a and is assumed to propagate directly towards Earth. With a choice of v_i the acceleration is therefore constrained kinematically by the observed event duration over the distance of 1 AU.

The type II dynamic spectrum $T(t, f)$ is calculated by summing the flux of radio emission from all ripples over the global shock [*Knock et al.*, 2003a, b; *Knock and Cairns*, 2005; *Florens et al.*, 2007; *Hillan et al.*, 2012]. The four main steps leading to radio emission [*Knock et al.*, 2001] in the foreshock are: (i) Shock-drift acceleration of electrons at the macroscopic, rippled, paraboloidal shock front as it propagates through the plasma. (ii) Formation of electron beams in the foreshock region upstream of the shock due to restrictions on the parallel velocity of reflected electrons [*Filbert and Kellogg*, 1979; *Cairns*, 1986, 1987]. (iii) Growth of Langmuir waves due to an electron beam instability and persistence of the available free energy due to stochastic growth effects [*Robinson*, 1992; *Robinson et al.*, 1993; *Cairns and Robinson*, 1999]. (iv) Nonlinear decay and coalescence processes of Langmuir waves lead to radio waves at f_p and $2f_p$ [*Melrose*, 1985; *Cairns and Melrose*, 1985; *Cairns*, 1988; *Knock et al.*, 2001; *Hillan et al.*, 2012].

The theory predicts that the emitted radiation's intensity and frequency-time structures depend sensitively on the shock's 3D location, velocity, and (upstream) emitting volume and associated solar wind parameters, and not just on the shock speed. Reasons include: (i) the emitted flux for each ripple or for the macroscopic shock depend on the respective radius of curvature squared [*Knock et al.*, 2003a]); (ii) the macroscopic shock's radius of curvature R_c and emission volume depend on s, d, and h via (2) while the local ripple radius of curvature $r_c(h)$ varies with h according to (1); (iii) specific frequency-time components are only produced when the relevant solar wind regions are within the shock's emission volume [*Knock and Cairns*, 2005; *Cairns and Knock*, 2006; *Florens et al.*, 2007]; (iv) the time-evolving shape of the macroscopic shock will alter the local angle θ_{UB} of a ripple and so the radiation flux [*Knock et al.*, 2003a] while (v) changing the shock's velocity and acceleration profiles will alter the relative velocity between each ripple and the local solar wind, and so the radiation flux [*Knock et al.*, 2003a]. Finally, (vi) localised solar wind structures within the active emission volume upstream of the shock are responsible for much of the variability and structure in the radio emission [*Reiner et al.*, 2001; *Cairns et al.*, 2003; *Knock and Cairns*, 2005; *Cairns and Knock*, 2006; *Florens et al.*, 2007]. Accordingly V_i, s, d, and a model for the inhomogeneous solar wind plasma are all important quantities for a truly quantitative theory of type II emission that attempts to describe and fit the levels and fine structures in observed dynamic spectra, as considered here.

The Wind/WAVES data are conventionally displayed in decibels (dB) of the total intensity relative to the minimum total daily background (instrument and natural signals), e.g., [*Bougeret et al.*, 1995; *Kaiser et al.*, 1998; *Reiner et al.*, 1998; *Bale et al.*, 1999]. Here, the standard Wind/Waves approach is adopted: a detailed model for the intensity $B(f)$ of background signals is added to $T(t, f)$, and this combined intensity is then divided by

$B(f)$ and converted into dB; i.e.,

$$\mathrm{DB}_T(t, f) = 10\mathrm{log}[(\mathrm{T(t,f)} + \mathrm{B(f)})/\mathrm{B(f)}]. \quad (3)$$

This process yields the spectrum $DB_T(t, f)$ which is appropriate for direct comparisons between theory and observation. In this way, the observations remain unaltered, the effects of the instrumental and natural backgrounds on the observability of the type II radiation are included, the analyses are performed with data that are routinely and rapidly available (as desired for the desired space weather applications), and both the data and theoretical predictions are given in dB as type IIs are typically weak compared with the observed satellite background.

The background model of *Hillan et al.* [2010] is used to predict $B(f)$ as a function of frequency (in W m^{-2} Hz^{-1}) over the entire frequency range of the Wind/WAVES instrument (4-13825 kHz *Bougeret et al.* [1995]). This model includes contributions from galactic background radiation, dominant at high frequencies above around 300 kHz, local quasithermal plasma noise, dominant at low frequencies below around 300 kHz, and receiver noise. The dynamic spectrum $DB_T(t, f)$ in dB is calculated with a time resolution of 1 minute. It can now be directly compared with those measured by Wind/WAVES and reported in dB as $DB_O(t, f)$ by the Wind/WAVES team (e.g., *Bougeret et al.* [1995]; *Kaiser et al.* [1998]; *Reiner et al.* [1998, 2001]). All simulation results presented in this paper are in these units. Future work should evaluate the effects of the logarithmic compression into a dB scale and the possible benefits of converting the observations into calibrated intensities in absolute units and then performing the theory-data comparisons.

To compare the observed and theoretical dynamic spectra we perform a cross correlation of the two images. This yields an array of correlation coefficients $C(t, f)$, where we label the maximum correlation coefficient $C_{\max}$. The time and frequency index at which $C_{\max}$ occurs is labeled the "offset" (t_0, f_0), where t_0 is number of time steps (min) and f_0 is the number of frequency channels relative to the centre. We use 550 frequency channels consistent with the frequency spacing and range of the Wind/WAVES instrument [*Bougeret et al.*, 1995] in order to allow direct comparisons between theory and observations. In the range where much of the observed type II emission occurs (typically $\approx$ 20 kHz - 1 MHz), the frequency spacing is normally no greater than 4 kHz [*Bougeret et al.*, 1995]. We combine (t_0, f_0) into a quantitative figure of merit

$$\alpha = \sqrt{\left(\frac{t_0}{n}\right)^2 + \left(\frac{f_0}{m}\right)^2}. \tag{4}$$

Then α is a dimensionless measure of the distance the two images are offset and must be translated to attain maximal agreement [*Hillan et al.*, 2012]. Another figure of merit is the value of $C_{\max}$ which is independent of α and is used below.

Another way to quantitatively compare the observed $DB_O(t, f)$ and theoretical $DB_T(t, f)$ dynamic spectra is to calculate the sum of the normalised difference at each point, i.e.,

$$\beta = \sum_{i=1}^{n} \sum_{j=1}^{m} \frac{|DB_{Ti,j} - DB_{Oi,j}|}{DB_{Ti,j} + DB_{Oi,j}}, \tag{5}$$

where n and m are the number of time and frequency points, respectively. The quantity β measures the total normalised difference in flux levels between the two data sets at every point in $f - t$ space. Reducing this parameter should increase the agreement between two data sets, as demonstrated for synthetic type II dynamic spectra [*Hillan et al.*, 2012].

The shock parameters yielding the best agreement between theory and observation are then extracted by iteratively minimising either α or β via a downhill simplex "Amoeba" method [*Nelder and Mead*, 1965; *Press et al.*, 1992]. This method requires a starting simplex with $(n+1)$ vertexes, where n is the number of shock parameters to be fitted and the vertex parameters are chosen within plausible ranges shown in Table 1. The value of α or β is calculated for each initial vertex and the algorithm then seeks to minimise these values and converge to a minimum (defined to be when the values agree to within 5%). The scheme is repeated multiple (up to 20) times with new randomly chosen vertices in the starting simplex to help avoid convergence to local minima and not the global minimum. This method has been tested and found to be successful in extracting shock parameters for artificial type II events generated with realistic model solar winds [*Hillan et al.*, 2012].

Future work may find more robust and effective optimisation schemes and figures of merit. However, parameters like β that measure the absolute deviation are expected to be more robust than the χ^2-statistic [*Press et al.*, 1992], in part since the probabilistic interpretation of the χ^2 statistic formally requires the deviations to be normally distributed, which is often not true. For instance, fluctuations in the galactic background and receiver noise observed by the Cassini Radio and Plasma Wave Science instrument at 1.075 MHz are not exactly Gaussian (Figure 3c of *Zarka et al.* [2004]): the distribution has two peaks near the core and significantly non-Gaussian tails. Similarly, non-Gaussian errors or uncertainties are expected in the predicted type II dynamic spectrum due to the different positions of ripples between iterations (and even between the Amoeba vertices for a given iteration). The focus of this paper and its companion is not on numerical algorithms but instead on testing the theory for type II bursts and on effective iterative data-theory fitting. The results of these papers demonstrate that the techniques used are effective and robust.

3. Type II Observations

This section summarizes observations of three relatively well-observed type II bursts. The chosen events are relatively strong and continuous with data from additional instruments available to constrain or estimate event parameters. Relevant observations here include the radio dynamic spectra, the time of arrival and properties of the shock measured by spacecraft in the solar wind, and CME data.

CMEs may be imaged using white light coronagraphs such as those found on the Large Angle Spectrometric COronagraph (LASCO) onboard the Solar and Heliospheric Observatory spacecraft (SoHO). The three coronagraphs C1, C2, and C3 image the corona in their field of view (fov) from 1.1 to 30 $R_\odot$ [*Brueckner et al.*, 1995]. C1 was disabled in June 1998, restricting LASCO's fov to the range 1.5 to 30 $R_\odot$. LASCO observations allow the tracking of the white light CME to create height-time plots. With sufficient observations in LASCO's fov, a second order fit to the height-time plots may be used to estimate the initial speed v_i and acceleration a of the CME [*Yashiro et al.*, 2004] and so the associated shock. Events with only two height-time observations allow only a first order speed estimate.

The WAVES instrument on board the spacecraft Wind is designed to record radio and plasma waves in situ from 4 kHz to 13825 kHz, especially those related to solar and interplanetary radio emissions [*Bougeret et al.*, 1995]. Observed type II solar radio bursts are recorded as intensities relative to the spacecraft's observed radio background as a function of time and frequency $O(t, f)$, plotted in dB as the dynamic spectrum $DB_O(t, f)$ defined similarly to (3). (A factor of 10 in the factor $(O(t, f) + B(t, f))/B(t, f)$ then corresponds to a difference of 10 dB in $DB_O(t, f)$.) A model for the WAVES instrument's observed background, including galactic background radiation and quasithermal plasma noise from the solar wind plasma, is presented in *Hillan et al.* [2010] and used here. The dynamic spectra $DB_O(t, f)$ plotted in Figure 2 are all measured in dB relative to the observed radio and instrument background as per (3).

On 3 December 2004, LASCO observed a full "halo" CME at approximately 00:26 UT, initially on the C2 coronograph (LASCO/SOHO CME catalog [*Yashiro et al.*, 2004]). Figure 1 contains a panel showing the initial LASCO CME observation and evolution. The CME-driven shock arrival at Earth may be seen in Wind spacecraft data at 04:30 UT on 5 December 2004, 3126 minutes (min) after the initial CME event. The second order LASCO acceleration and speed estimates leads to an initial CME speed of $v_i = 1350$ km s^{-1} and acceleration of $a = -19$ m s^{-2}, both in the plane-of-the-sky.

Type II emission resulting from the CME on 3 December 2004 was observed by Wind/WAVES and is displayed in Figure 2 (top left). The quickly drifting type III emission at high frequencies that occurred early during the event has been removed and set to 0 dB. Some interference signals and emissions at frequencies above the drifting type II emission have also been removed. This event is an excellent example of an interplanetary type II, with bands of emission that drift down all the way to the local plasma frequency at Earth ($\approx$ 24 kHz) and little evidence of interference from auroral kilometric radiation (AKR) in the range 100 to 500 kHz.

Another relatively well-observed type II event started on 13 May 2005 with a CME first observed at 17:12 UT [*Yashiro et al.*, 2004]. The shock arrived at Earth on 15 May at 02:08 UT after 1976 min. Only two initial LASCO coronograph observations of the CME are available, leading to two data points on the height-time plots. The observations suggest that the event was "halo" like with a first-order estimated speed $v_i = 1690$ km s^{-1} in the plane-of-the-sky. Figure 2 (top right) plots the observed dynamic spectra after removing some unwanted non-type II emission. However, the bright emission after 1200 min at around 50-200 kHz is possibly interference from AKR. Figure 2 (bottom left) plots the same event with the possible AKR signal set to 0 dB. With these two observational data sets we can compare the theory and observation to assess whether the high frequency emission is actually AKR or part of the type II burst.

On 24 August 1998 at 22:09 UT a CME was observed to produce the interplanetary type II studied by *Bale et al.* [1999]. The shock arrived on 26 August at 06:39 UT after 1950 min. Unfortunately SOHO was unavailable during August 1998. However, *Bale et al.* [1999] estimated $v_i = 1300$ km s^{-1} by assuming that the shock had approximately constant speed from formation to arrival at Earth ($a = 0$ m s^{-2}). The dynamic spectrum for this event is plotted in Figure 2 (bottom right).

4. Initial comparisons between theory and observation

Here we simulate the dynamic spectra for the three observed type II events using (i) estimated shock parameters taken mostly from LASCO/SOHO observations and (ii) solar wind models generated using Wind spacecraft data for the solar rotation period before each shock reached Earth [*Florens et al.*, 2007]. The LASCO/SOHO shock velocity estimates are made via the plane-of-the-sky observations. While more realistic radial speeds may be obtained through analyses such as those by *Schwenn et al.* [2005] and *Michalek et al.* [2009], we use the LASCO/SOHO estimates as a first guess. The assessment parameters α and β from (4) and (5), respectively, and $C_{\max}$ are calculated by comparing each simulated spectrum with the observed satellite data in Figure 2. Each simulated dynamic spectra has 550 frequency channels that match the frequency range (4-13825) kHz and spacing of the Wind/WAVES instrument, with a one minute time resolution (i.e. 3126, 1976 and 1950 points in time for the 3 December 2004, 13 May 2005, and 24 August 1998 event, respectively).

4.1. 3 December 2004 event

For the 3 December 2004 event, the initial shock speed is set to $v_i = 1350$ km s^{-1} based on the LASCO/SOHO data, with the arrival time at Earth then constraining the average CME deceleration to be $a = -5.8$ ms^{-2} over the entire Sun to Earth transit. Note that the LASCO/SOHO acceleration estimate $a = -19$ ms^{-2} is valid only to 20 $R_\odot$. We set parameters $s = 1.0$ and $d = 0.00$ in (2) to approximate a large halo-like shock (the radius of curvature will equal 1 AU when $h = 1$ AU) whose size expands linearly with heliocentric distance. The solar wind model is shown in Figure 9 of Section 5 of *Hillan et al.* [2012]. The resulting dynamic spectrum is shown in Figure 3 (top left) with the fundamental and harmonic emission labeled.

Comparison by eye of the predictions in Figure 3 (top left) and observations in Figure 2 (top left) shows reasonable semiquantitative agreement in the location of emissions in time and frequency. The primary fundamental band (the higher frequency band marked with F) and the intermittent band that is a mixture of fundamental and harmonic emission (F+H) both start near $t = 500$ min, similar to the observed data. The observed data has some bright spots in the fundamental band at around 10-20 dB with the bulk of the emission from both bands lying in the 5-10 dB range. This agrees well with the predicted primary fundamental band, with agreement in emission intensity, time, and frequency of some bright spots, for example the spot occurring at ≈ 1800 min and 50 kHz. The intensity of the predicted (F+H) band overpredicts the emission by as much 10 dB and only agrees well with the timing and frequency range of the observed upper band until around 2000 min. At this time in the observational data the lower and upper bands reappear, with the fundamental band reappearing with more intensity, after having faded out for around 300 min. However, this is only consistent with the predicted fundamental band of the which agrees well with the observed timing and intensity levels. The predicted upper harmonic (H) band occurs in a frequency range that has been removed in the observation dynamic spectrum and hence has no counterpart for comparison, and a very weak lower fundamental band is also predicted. Both the observation and simulation show emission that is bursty and intermittent, with some bright spots that correspond closely.

Continuing with qualitative aspects, Figure 3 does show that the models (for all three events) typically have several more emission bands than are actually observed. However, most of these additional bands are very weak, being less than 5 dB above the noise background (meaning the sum of the receiver, quasi-thermal plasma noise, shot noise, galactic background radiation, and any other natural radio signals). This degree of agreement without any optimization should be considered good for a first quantitative test of the theory. Even so, since these additional bands would be detectable and since they often persist after the optimization processes in Section 5, this aspect of the data-theory comparisons is addressed specifically in Section 6.

To quantify the agreement between theory and observation, a normalised cross-correlation of the dynamic spectra is performed, yielding an array of correlation coefficients $C(t, f)$. The maximum correlation coefficient is 24% (i.e., $C_{\max} = 0.24$) with time and frequency offsets (t_0,f_0) of 77 min and 5 frequency channels (< 20 kHz), respectively, corresponding to $\alpha = 2.63 \times 10^{-2}$. This correlation coefficient implies reasonable agreement between observation and the simulation (which uses shock parameters estimated from LASCO/SOHO and no optimization): similar correlation co-efficients of 25-40% are found when comparing synthetic dynamic spectra in the companion paper [*Hillan et al.*, 2012]. The offset of around 1 hour in time highlights the fact that the main bands of emission in the theory and observation do not occur at exactly the same time and frequency. However, it is relevant that this time offset is only $77/3126 < 3\%$ of the event duration, implying good agreement. Similarly, a frequency offset < 20 kHz for a characterisitc frequency (100 to 200 kHz) is better than 20% accuracy. The β value for this simulation is calculated to be 2.88×10^5. These two measures are used in the iterative scheme below to improve the agreement between observations and theory.

4.2. 13 May 2005 event

The 13 May 2005 event is simulated using the parameters $v_i = 1690$ km s^{-1}, $s = 1.0$, and $d = 0.00$ derived from LASCO/SOHO observations. The shock arrival after 1976 min constrains the acceleration to $a = -7.2$ m s^{-2}. The solar wind model is shown in Figure 4. The predicted dynamic spectrum is shown in Figure 3 (top right) with the fundamental and harmonic emission labeled. We firstly consider qualitative comparisons with the observed dynamic spectrum in Figure 2 (top right and bottom left), which contains broad emission that starts at around $t = 400$ min and persists until the shock reaches Earth, with relative flux levels at around 5 to 10 dB. The observed emission initially appears fairly consistent but does contain spots of brighter emission in the main band after around 1000 min that range up to 15 - 20 dB in relative flux. There is also strong (30 dB or above) bursty emission observed at times after about 1200 min and frequencies of about 50-200 kHz. As discussed above, some or all of this emission may be AKR and comparisons with and without this emission excised are discussed below.

As in the observations in Figure 2 (top right and bottom left), the prediction in Figure 3 (top right) shows the main harmonic (F) band also starting at around 400 min and continuing throughout the event, with the bulk of the emission level not inconsistent with the observations at around 5 dB. The emission in the predicted fundamental band weakens from around 1000 to 1400 min and then begins to intensify with some bright spots at around 1500 min and onwards of 5 - 10 dB. This is not inconsistent with the main band in the type II observation. The predicted harmonic band (H) begins at around 900 min and is very intermittent until 1400 min when it broadens and intensifies up to 5 - 10 dB. This is consistent with and corresponds closely in time and frequency with the bursty emission that begins in the observation at around 900 min and 200 - 300 kHz. However, the brightest spot in the observation reaches almost 50 dB, well above the ≈ 10 dB in the prediction. Thus, the theory's successful predicion within $5 - 10$ dB of both the main emission band and some of the patchy higher frequency emissions suggests that, at the least, some of the higher frequency emission in Figure 2 (top right) is type II emission and not AKR.

Cross-correlation of the data in Figure 2 (top right) for the 13 May 2005 event (including the possible AKR) with the theoretical predictions, yields a maximum correlation coefficient of $C_{\max} = 0.32$ with $(t_0, f_0) = (64, 23)$ so that $\alpha = 5.29 \times 10^{-2}$. This implies reasonable agreement in the structure of the simulated and observed type II burst, albeit with a ≈ 1 hour shift in time between observation and theory. The time offset corresponds to $\approx 3\%$ of the event length and the frequency offset to around 80 kHz which is within a factor of two of the characterisitc emission frequency of 100 to 200 kHz. The β value for this simulation is calculated to be 1.64×10^5.

We repeat the quantitative assessments for this event, except we now use the type II data with the possible AKR source removed (as in Figure 2 [bottom left]). Cross-correlation yields a maximum correlation coefficient of $C_{\max} = 0.25$ with $(t_0, f_0) = (672, 16)$ so that $\alpha = 3.41 \times 10^{-1}$, while we calculate $\beta = 1.12 \times 10^5$. The strength of the match is therefore decreased, as evidenced by a decrease in $C_{\max}$ and a large increase in α, whilst the β parameter has improved by $\approx$30%. It is not unreasonable to assume that only some, and not all, of the strong intermittent emission seen in Figure 2 (top right) between 50 - 200 kHz from time 1200 min onwards is AKR, since our model predicts some emission in this range and inclusion of this emission leads to stronger agreement between theory and observation for two of our three agreement measures when using the shock parameters estimated from LASCO/SOHO data.

4.3. 24 August 1998 event

The 24 August event is simulated using the parameters $v_i = 1300$ km s^{-1}, $s = 1.0$, and $d = 0.37$ estimated from *Bale et al.* [1999] and *Florens et al.* [2007]. The shock's transit time to 1 AU of 1950 min constrains $a = -0.4$ m s^{-2}, which implies a shock speed that is close to a constant. The solar wind model is shown in Figure 5. Figure 3 (bottom left) displays the predicted dynamic spectrum with the fundamental and harmonic emission labeled. The observed spectrum in Figure 2 (bottom right) contains mostly broadband emission at levels of 5 to 10 dB. However, there is some strong emission at 10 to 20 dB that occurs for times 200 to 500 min, with one spot reaching almost 30 dB. There are also some bright spots at around an elapsed time of 800 min near 200 kHz after which the emission narrows in frequency span and decreases in intensity. Approaching 1600 min, the intensity increases again with an obvious spot with enhanced surrounding emission at around 1900 min.

The predicted spectrum in Figure 3 (bottom left) contains multiple drifting bands with emission over many frequencies simultaneously, some of which are strong and/or bursty. Several fundamental (F) and harmonic (H) bands are evident, some of which are superposed, with the harmonic bands being the brightest. The bulk of the emission in the drifting bands is at around 10 to 20 dB with overlying bright bands of 25 dB. The predicted upper harmonic bands fade out by around 800 min which is consistent with the narrowing and fading of the large region of emission observed. The relative flux levels differ here however, with the theory overpredicting the levels of emission by around 10 dB. The predicted emission narrows between 800 to 1400 min consistent with observation, but again the flux levels are around 20 dB too high. Finally, the predicted emission broadens and intensifies, as found in the observation, but with multiple blobs of emission at around 20 - 25 dB rather than the observed fluxes of $\approx 10 - 15$ dB. Qualitatively, the transition from broad intense to narrow weakening emission, followed again by a broad intense emission is predicted by theory with times and frequencies that agree well with observation. The predicted relative flux levels are, however, significantly higher than those observed.

Cross correlation of these two spectra yields $C_{\max} = 0.37$, along with significant time offsets $(t_0, f_0) = (193, 0)$ giving $\alpha = 9.90 \times 10^{-2}$. The time offset is $\approx$10% of the event duration. This confirms the qualitative view that the general pattern of the predicted emission is consistent but that the agreement of the times and frequencies of spectral features may be improved. The β value is calculated to be 2.14×10^{5}. As has been observed in some cases with the events investigated above, the relative flux level of the predicted emission is generally too high when compared with the observed type II event.

5. Iterative comparisons between theory and observation and extracted parameters

The Amoeba downhill simplex (optimisation) method is now used to constrain the shock parameters for the three type II events studied. This is performed using (4) or (5) to measure and compare the agreement between the simulated and observed dynamic spectra, and then to iteratively minimise this assessment parameters. Model shock parameters are randomly chosen in the ranges shown in Table 1 to form the vertexes of the starting simplex. Convergence is obtained when the simplex values of α or β differ by 5% or less. The process is repeated for multiple (up to 20) initial starting simplexes. The results from these analyses and those in the last section are summarized in Table 2 with the first column stating which comparative method was used to extract the displayed parameters.

5.1. 3 December 2004 event

LASCO/SOHO observations are able to constrain the CME's initial speed in the plane-of-the-sky, which may differ significantly from the initial radial speed v_i. Hence we extract the shock's initial radial speed v_i, size s, and expansion index d using the iterative optimisation method with initial parameter estimates randomly chosen in the ranges shown in Table 1. The results are in Table 2.

Iteratively minimising the quantity α, defined by (4), yields $\alpha = 9.10 \times 10^{-3}$, $(t_0, f_0) = (1, 5)$, and correlation coefficient of $C_{\max} = 0.24$. The parameters found are $v_i = 1423 \pm 1$ km s^{-1}, $a = -6.7$ m s^{-2}, $s = 1.1 \pm 0.01$, $d = 0.42 \pm 0.01$ for the dynamic spectrum shown in Figure 6 (bottom left). These parameters are within 30% of those estimated from

LASCO/SOHO observations of the associated CME and the strong similarities may be seen in Figure 6 (top right), which plots the location and evolution of the model shocks at various times. Minimising the α parameter has extracted a solution with a larger initial radial velocity and larger global radius of curvature that expands more rapidly than the initial estimates. This solution has a consderably smaller time offset t_0 with no change in the $C_{\max}$ value. Note that these offsets are $< 1\%$ and $< 20\%$ of the event's duration and characteristic frequency, respectively. The β value is calculated to be 2.86×10^5 which is only slightly smaller than for the initial LASCO/SOHO shock parameters in Section 4.1.

Iteratively minimising the quantity β, defined by (5), yields $\beta = 2.76 \times 10^5$ with $v_i = 1490 \pm 6$ km s^{-1}, $a = -7.4$ m s^{-2}, $s = 0.6 \pm 0.1$, $d = 0.35 \pm 0.02$, and the dynamic spectra shown in Figure 6 (bottom right). Iterative fitting has therefore reduced β by 4%. The values of α and C_{max} for this solution are 1.86×10^{-2} and 0.18, respectively, which is an improvement in the size of the offsets but a decrease in the strength of the correlation. The s and d parameters are again within around 30% of the LASCO/SOHO estimates but this time with a smaller radius of curvature. Figure 6 (top right) shows the strong similarity between the α solution and the LASCO/SOHO estimates, whereas only the nose of the β solution tracks the other two closely with its flanks closer to the Sun.

Similar to the initial simulation in Figure 3 (top left), based on the LASCO/SOHO shock parameters, the α optimised solution predicts two strong bands of emission that agree well with the observations. The α solution's drift rate has steepened due to the increase in velocity and hence the spectral features have shifted towards earlier times to increase agreement. It is this which has reduced the time offsets from 77 to 1 min. However, some emission is now predicted before 500 min, which is not observed. The change in velocity has also led to broadening in emission and some intensifications that, while corresponding well in time and frequency, are at flux levels too high compared with observation. The increased relative flux levels occur mostly at early times and gradually shift back into alignment with the earlier LASCO/SOHO simulation. As for the LASCO/SOHO shock parameters, the α solution predicts a weakening in the two main bands with the fundamental band re-appearing with a bright spot near 2000 min that continues until the end.

The smaller radius of curvature for the β solution has led to a narrowing in emission in time and frequency and hence a removal of most of the very intense bright spots. No emission is predicted before around 600 min as per the observations and the lower weak fundamental band evident in the LASCO/SOHO observation has disappeared. Where emission is predicted it is typically within 5 dB of the observed values. However, an upper harmonic band is still predicted at around 500 kHz which is outside the domain of the observational data considered. This confirms that the β solution is more effective at matching the relative flux levels of the bulk emission that the α solution. The values of the parameters for the initial LASCO/SOHO estimates and the α and β solutions lie within 30% or better of each other. This suggests that the LASCO/SOHO CME observations provide a reasonable estimate of the shock paramters, and that the type II theory generates dynamic spectra with reasonable semi-quantitative agreement with observation.

5.2. 13 May 2005 event

Limited SOHO observations of the associated CME suggest that v_i for this event is 1690 km s^{-1}. This estimate is in the plane-of-the-sky and is based only two data points being available; the actual speed may differ significantly from this estimate. Accordingly, the three parameters (v_i, s, d) are extracted using the optimisation methods. The initial vertexes are chosen randomly in the parameter ranges shown in Table 1. The results are in Table 2.

Using the optimisation method to minimise (4) gives $\alpha = 3.64 \times 10^{-2}$ with $(t_0, f_0) = (0, 20)$ and a maximum correlation coefficient of $C_{\max} = 0.33$ when calculated using the observational data from Figure 2 (top right), also shown in Figure 7 (top left). The parameters found are $v_i = 1515 \pm 5$ km s^{-1}, $a = -4.3$ m s^{-2}, $s = 2.9 \pm 0.1$, $d = 0.37 \pm 0.01$ and the resulting spectrum is plotted in Figure 7 (bottom left). The shock shape is broader and slower than the initial model in Section 4.2, as seen in Figure 7 (top right). This new model shock leads to improved time offsets, hence reducing the α parameter, but worse frequency offsets with little change in $C_{\max}$. The β parameter is calculated to be 1.59×10^5, which is a reduction compared with the initial model.

Compared with the prediction based solely on the LASCO/SOHO estimates, the iterated α solution has a slight increase in the relative flux level of the bulk of the emission in frequency. The most prominent effect of minimising α has been to significantly broaden the emission, especially the harmonic emission at high frequencies, as we might expect for a model shock with a more planar profile. The predicted fundamental band starts at around 500 min and agrees well in intensity and timing with the main observed band until around 800 min. The predicted band is, however, at a lower frequency, as evidenced by the still relatively large frequency offset in the α solution. At around 800 min, the predicted spectra broadens and intensifies which agrees well with the observation. The relative flux levels of both the bulk emission and the brighter spots agree mostly to within

10 dB or better. Some of the higher predicted harmonic bands then fade out, weaken, and narrow at around 1700 min which also agrees well with observation. There is also a correspondence between the brightest predicted spot of about 25 dB with the timing of that seen in the observation at around 1300 min, albeit with a frequency difference of around 20 kHz.

Using the optimisation method to minimise (5) gives $\beta = 1.56 \times 10^5$ and a maximum correlation coefficient of $C_{\text{max}} = 0.35$ with $\alpha = 3.83 \times 10^{-2}$ when calculated using the observational data in Figure 2 (top right) also shown in Figure 7 (top left). This shows an improvement in all the assessment metrics with extracted parameters $v_i = 1385 \pm 2$ km s^{-1}, $a = -2.1$ m s^{-2}, $s = 3.0 \pm 0.1$, $d = 0.15 \pm 0.02$. This is a reduction in β by a factor of 5.7. The dynamic spectra for this iterated fit is shown in Figure 7 (bottom right). The shock's time evolution is plotted in Figure 7 (top right) for comparison. The evolution of the β extracted shock tracks that of the α shock very closely, but has a slightly slower velocity and slightly broader shock shape.

Since the α and β shock solutions are so similar, their dynamic spectra contain many similar features. The main difference is the extension of the fundamental bands to before 500 min in the β solution. The predicted lower fundamental band starting at 100 min and 200 kHz corresponds closely in time, frequency, and intensity to the emission seen in the observation. The predicted higher fundamental band that starts at around 400 min agrees well with the timing of the onset of the main band in the observation. In both the extracted solutions, the bulk of the emission agrees to within about 5 dB of the observations, with semi-quantitative agreement with observed spectral features. In this case both solutions converged to broader and slower model shock parameters than those estimated from the associated CME observations.

5.3. 24 August 1998 event

There is no constrained initial speed for the associated CME for this event and so we extract the three parameters (v_i, s, d) using the optimisation method, again using randomly chosen vertexes in the ranges shown in Table 1. The results are in Table 2.

Using the optimisation method to minimise (4) gives $\alpha = 3.64 \times 10^{-2}$ with $(t_0, f_0) = (0, 2)$ and a maximum correlation coefficient of $C_{\rm max} = 0.39$ when calculated using the observational data in Figure 2 (bottom right) also shown in Figure 8 (top left). This shows a large improvement in the strength of agreement and in reduced offsets compared with the initial prediction. The parameters extracted are $v_i = 1980 \pm 1$ km s^{-1}, $a = -12.0$ m s^{-2}, $s = 2.3{\pm}0.1$, $d = 0.83{\pm}0.01$ and the resulting spectrum is plotted in Figure 8 (bottom left). This solution has $\beta = 2.11 \times 10^5$ which is also an improvement over the original model. Similarly using the optimisation method to minimise (5) gives $\beta = 2.10 \times 10^5$ with the parameters $v_i = 1592 \pm 1$ km s^{-1}, $a = -5.4$ m s^{-2}, $s = 3.4 \pm 0.2$, and $d = 0.24 \pm 0.01$. The dynamic spectrum for this optimised fit is shown in Figure 8 (bottom right). This solution has only a small decrease in β but also has improved values of α and C_{max}, calculated to be 7.06×10^{-2} and 0.39, respectively.

The two extracted shock solutions are plotted in Figure 8 (top right). They are not mutually consistent in detail although they both show extremely broad shocks at a much higher velocity than that which was assumed earlier based on a constant velocity model. The broad shocks span large regions of the solar wind and generate broadband emission with multiple bright bands. Both the α and β methods have converged to a solution that attempts to move a large amount of predicted emission into the time period 200 to 800 min and frequency range 50 to 200 kHz, which has a counterpart in the observed type II (Figure 8 [top left]). The relative flux levels of these emission regions are around 10 dB or more higher than those which are observed. Although the extracted solutions are successful at predicting emission before a time of 700 min that is mostly absent in the initial simulation of Section 4.3, the observations show a drop in flux and a narrowing in frequency after around 800 min that is not evident in the extracted spectra. The simulated broad emission bands continue after this time and significantly overpredict the observed emission levels, with patterns and features that mimic Figure 3 (bottom left) but with differing drift rates.

6. Discussion

The results of Section 4 show reasonable agreement between the type II simulations and the observed data. We obtain 25-40% correlation coefficients when using the initial and fitted shock parameters. Many of the features in the spectra agree semiquantitatively with the observations. Where there exists differences in time and frequency between the predicted features and those observed, this determines the size of the offsets and hence the sizes of α and β. In general the relative fluxes predicted theoretically appear too high compared with the observations, as discussed more below, and this leads to substantial values of β (offsets in time and frequency also contribute to β). In the case of the extracted solutions for the 13 May 2005 event, the α and C_{max} values improved when calculated using the data that include the possible source of AKR, whilst the β value increased (Figure 2 [top right]). This implies that, at at least, some of the observed high frequency emission is indeed type II radiation.

The dynamic spectra predicted in Figures 3 and 6-8 show little evidence for emission above 1 MHz, although the such emission is observed in Figure 2 for at least the 24 August 1998 event. The most plausible reason for this is the solar wind-like (and so primarily radial) magnetic field mode used. Such field orientations make the shock quasi-parallel at the nose and so relatively poor at producing radio emission [*Knock and Cairns*, 2005; *Cairns*, 2011]. Alternatively, the shock may need to expand more transverse to these quasi-radial fields to excite radio emission. Detailed attempts to understand coronal type II bursts will require more detailed modeling of the magnetic fields and of the 3D shock location and motion *Cairns* [2011].

In Section 5 the optimisation method successfully reduced the time and frequency offsets by minimising the quantity α, leading to improved alignment of spectral features and extraction of the model shock parameters. Time offsets were typically observed to be tens of minutes, which is very encouraging since aligning the start of the simulation with the observed event onset may only be reasonably considered accurate to with around 10 minutes. These values are typically less than 5% of the event duration. The frequency offsets were typically less than 20 units ($\approx$ 4 kHz each) and hence we may estimate an average frequency shifting difference of less than 80 kHz (see Section 2) and so $<$ 50% of the characteristic radiation frequency. For much of the observed frequency range this is small. One implication is that our solar wind density model is accurate to within a factor of 2 or better. These offsets are very reasonable.

Applying the minimisation methods to the 3 December 2004 event led to two slightly different extracted solutions, both of which track fairly closely to the shock estimated from the observations. The α solution improved the alignment of the predicted bright spots in time and frequency with those in the observation, whereas the β solution minimised the amount of predicted emission occurring outside of the observed time and frequency range and matched the emission levels more closely. Typically, however, the theory seems to overpredict the emission in the bright spots by around 5 - 10 dB (or a factor of $\approx 3 - 10$ in intensity).

Figure 9 provides new assessments for the agreement between the observed type IIs and the theoretical predictions for all three events. It shows the mean and peak fluxes in dB relative to the background as a function of frequency; e.g. a value of 10^0 means 1 dB. For the 3 December 2004 event, the observations and predictions generally agree to within 5 to 10 dB in peak flux and a few dB in mean flux. In detail, the overprediction in peak flux can be seen clearly at high frequencies (above 100 kHz) in the first row of Figure 9. This Figure also verifies that the β solution reduces the difference between the observation and simulations in terms of the peak flux. Furthermore, the plot of the mean flux as a function of frequency shows the simulated values to be smaller than the observed values due to the simulated emission appearing more narrow band than what is observed.

As raised in Section 4.1 in connection with Figure 3, an important qualitative aspect is that the non-optimised and optimised theoretical predictions in Figures 3 and 6-8 for all three events typically have several more emission bands than are actually observed. Most of these additional bands are weak, being less than 5 dB above the noise background, but would be detectable if present. Even so, the degree of quantitative agreement is surprisingly good for a first quantitative test of such a multi-process and multi-component theory. Nevertheless, the persistence of this qualitative aspect points to a need for possible modifications of the theory and its numerical implementation. It is relevant that the plasma parameters from the solar wind model are not currently smoothed or interpolated throughout the foreshocks of individual ripples and that density turbulence is not currently included. Neglect of these effects is intuitively expected to concentrate emission into restricted bands rather than spreading it in frequency and causing a more diffuse signal that might not be observable above the instrumental and natural background. In addition, differences between the true solar wind and the solar wind model, and between the assumed and actual distribution of ripples on the shock, will likely move emission in frequency and time (and flux). This will sometimes lead to bands that are not in the observations. Further work is required to see whether inclusion of smoothing/interpolation and turbulence effects removes the extra bands or whether other revisions of the type II theory and solar wind model are required to bring the theory and observations into better agreement.

Turning now to specific events, the optimised solutions for the 3 December 2004 event both support a large, halo-like, radius of curvature CME-driven shock, like that inferred from the CME observations, as they both converged to within 20-30% of the parameters estimated from CME observations (Figure 6 [top right]). Our results for this event show reasonable semiquantitative agreement with the predicted emission bands, bright spots, drift rate and flux levels of bulk emission. These results, using a constrained initial speed, imply very good consistency between the CME obsevations and the radio-derived shock model. This level of agreement (a few dB in mean flux and < 10 dB in peak flux) is very good for a first detailed comparison between observation and such a multiple process theory.

The differences in the α and β solutions for the 13 May 2005 event, despite their very similar shock evolutions, illustrate the sensitive dependence on the shock parameters of the resulting spectra. The plot of the mean fluxes in the second row of Figure 9 shows good agreement (to within a few dB) between the observations and predictions until around 100 kHz, after which the predictions fall well short of the bulge in the observed data (plotted as a solid black line). This bulge originates from the possible source of AKR, as discussed earlier in Section 4.2. The panel plotting mean fluxes shows how the β solution (plotted as green squares) is improved when compared with the observed data with the AKR excised (plotted as a dashed black line). The panel plotting the peak fluxes also shows the improved agreement between the β solution and the excised observed data. These sorts of comparisons highlight the need for well-observed "clean" observational data that are free from interference such as AKR, which may be achieved in the future by constraining the direction of the emission source. The plot of the peak fluxes show that while the optimised solutions can overpredict the flux at low frequencies (below 100 kHz) by up to tens of dB, they usually agree to within a few dB of the observation.

Both optimised solutions for the 13 May 2005 event also support halo-like shock solutions that are even broader than the initial estimates (Figure 7 [top right]). The initial speed is not well constrained by observations and both solutions extracted an initial speed that was lower than what we may expect from extrapolations of the two LASCO/SOHO CME height-time data points. The dynamic spectra for both solutions are similar and both predict the timing and flux levels of the bulk of the emission well, however generally at a slightly lower frequencies as evidenced by the frequency offset of around 20 units ($\approx 80kHz$). *Reiner et al.* [2001] found a large value of v_i (≈ 2500 km^{-1}) for this event and constrained the CME kinematics by tracking the drift rate. Their model involved CME deceleration only to 150 $R_\odot$, followed by a constant velocity. Incorporation of a radially varying CME deceleration may therefore allow this event to be modeled more accurately using the type II theory. However, the results here based on average deceleration, speed, and transit time estimates are promising for a first quantitative investigation.

The solutions obtained for the 24 August 1998 event by minimising α and β are consistent with one another in predicting a faster moving and broader shock than the initial model. Both confirm an initial shock speed well above the initial estimate of 1300 km s^{-1} that assumes zero acceleration, and both predict a large and planar-like shock (Figure 8 [top right]). Clearly the two methods have attempted to improve the agreement with the observed type II event by generating broad band emission at times 200-500 min and frequencies 50-200 kHz, achieved with a planar shock. This leads to good agreement between the predictions and observed data in terms of the mean flux, shown in the third row of Figure 9, where the agreement is generally to within a few dB. It can also be seen here that the optimised solutions (plotted as red crosses and green squares) with their broader shocks typically lead to an increase in the mean fluxes compared with the initial shock model prediction (plotted as blue dots) in the range of characteristic frequencies up to $\approx$ 200 kHz. The adjacent panel plotting peak fluxes verifies what is obvious by eye, that the peak predicted emission is much more intense (tens of dB difference), broadband, and persistent than observed.

Since the optimised solutions attempt to predict more emission at times 200 to 500 min and at frequencies 50 to 200 kHz for the 24 August 1998, it is possible that this may also be achieved by assuming a variable acceleration profile for the model shock as suggested for the 13 May 2005 event. For instance, an initially rapidly decelerating shock that changes to near zero deceleration later, as per the kinematics of *Reiner et al.* [2001], may produce the necessary drift rate and emission to improve the agreement without the need for such a planar shock. This narrower shock might then generate less emission in (t, f) space or less intense emission. Another possibility is that the enhanced emission for times 200-500 min and frequencies 50-200 kHz is interference by AKR and should be removed. This would be expected to lead to extraction of different shock models that predict no emission in this region.

While the combined type II theory predicts dynamic spectra that are in reasonable semiquantitative agreement with Wind observations, in terms of the level of emission and in the time and frequency occurrence of many (but not all) emission features, a number of limitations of the theory must be resolved before we should expect to make more accurate predictions, as reviewed in detail by *Cairns* [2011]).

First, the theory does not incorporate the effects of shock overshoots or non-stationarity, affecting the electron energization at the shock front. Inclusion of these effects is expected to increase emission by a factor of 2-4 [*Yuan et al.*, 2007].

Second, straight line propagation is currently assumed for the radio emission reaching a distant observer, ignoring the possibility of scattering from density irregularities and the effects of the radiation's intrinsic directivity patterns.

Third, the solar wind model [*Florens et al.*, 2007] needs to be revised as we currently assume persistence of solar wind stream structures over one solar period and, while θ_{Bn} (the angle between the shock normal and magnetic field) varies across each ripple and the macroscopic shock, the detailed modeling of the magnetic field is not fully self-consistent. The former point may be resolved by interpolating solar wind parameter observations from multiple spacecrafts i.e., STEREO A and B, and WIND [*Opitz et al.*, 2009]. The latter point involves more realistic modelling of the magnetic field by more consistently modelling the radial and azimuthal components [*Schulte in den Baumen et al.*, 2012]. This will likely alter where along the shock the most intense emission occurs, thereby slightly altering the predicted dynamic spectra.

Fourth, the richness in structure in the predicted dynamic spectra may be overestimated due to (i) not smoothing or interpolating the predicted solar wind properties from the model's heliolatitude - heliocentric distance grid to the location of each individual foreshock, (ii) ignoring turbulence in the solar wind, and (iii) again assuming persistence of solar wind structures as per the last point.

Fifth, repacking of the ripples of the global shock alters the location and duration of various spectral intensifications [*Knock et al.*, 2003b]. The magnetic decorrelation length determines the ripple lifetime in our simulations [*Cairns and Knock*, 2006], but more rigorous theoretical investigations need to be carried out to determine ripple lifetimes and more realistic ripple packing along the shock. Furthermore, the ripples are assumed to have azimuthal symmetry and therefore specify solar wind parameters out of the ecliptic which are different from those that would be predicted by our solar wind model for the same heliocentric distance. Ideally the azimuthal symmetry should be removed and a 3-D solar wind model implemented [*Cairns*, 2011].

Sixth, the direction of the shock with respect to Earth is likely important, whereas the current model assumes that the shock's vertex propagates directly Earthward. Altering the direction would change the dynamic spectra since the distance from the observer to the source region has increased or decreased and also because of frequency blocking effects [*Cairns and Knock*, 2006]. Initial calculations (not shown) confirm that this effect can be important.

Seventh, a more realistic shock evolution model would allow for non-constant or perhaps zero deceleration implemented at a certain heliocentric distance, consistent with observations [*Gopalswamy et al.*, 2001; *Reiner et al.*, 2001], and changes in the three-dimensional shock shape with heliocentric distance from a paraboloid. These extensions to the model may improve the predictions made for the 13 May 2005 or 24 August 1998 event, as mentioned above.

The net effect of resolving the above issues is unknown and constitutes future work for the development of the type II theory. It is hoped that extending and revising the theory will (i) make it more accurate and realistic, (ii) increase its ability to predict the location, burstiness, and intensity of spectral features, reducing the number of spurious bands, and (iii) allow the improvements to be quantified using the maximum correlation coefficient, the frequency and time offsets in α, and detailed quantitative quantities like β. The direction finding capabilities of the Wind and STEREO spacecraft may also be able to better constrain the shock's direction and to identify emission that is AKR. This information would improve our extraction of the shock parameters (as shown in Sections 5.2 and 5.3) and our ability to make quantitative comparisons between theory and observation. In addition,

Future work should also be performed to investigate possible improvements in the algorithms and implementation of the data-theory comparisons. These include evaluation of the effects of the logarithmic compression of the data and theoretical predictions onto a dB scale, the possible benefits of converting the observations into calibrated intensities in absolute units and then performing the theory-data comparisons, and alternative figures of merit and opimization schemes.

7. Conclusions

We have extended the type II model of *Knock et al.* [2001], *Florens et al.* [2007], and others to correctly include the observed spacecraft background in order to, for the first time, make quantitative comparisons between theory and observation for three relatively well studied type II events. Using LASCO/SOHO observations to guide our model shock parameters, we obtained reasonable agreement between theory and observation with maximum correlation coefficients of $\approx$ 25-40%, and reasonable semiquantitative agreement between numerous (but not all) features in our simulations and three relatively well-observed type II events. An investigation of possible contamination by AKR in the 13 May 2005 event determined that at least some of the emission was likely to be type II radio emission, since its inclusion in the observed data led to increased agreement with theory owing to prediction of spectral features at similar times and frequencies.

The α and β quantities were calculated for each event using the model shock parameters estimated from LASCO/SOHO observations and the arrival time at Wind. Through an iterative minimisation scheme, the agreement between theory and observation was improved and the associated shock parameters extracted. The parameters extracted define the initial shock speed, average acceleration, radius of curvature at 1 AU, and expansion index. Minimising both α and β resulted in convergence to similar parameters for each event. Furthermore, the extracted parameters led to model shocks that resembled those estimated from the LASCO/SOHO observations for the 3 December 2004. For the 13 May 2005 event, the extracted shock parameters were slower and more planar than our initial estimates, and for the 24 August 1998 event the parameters were again more planar but faster than our initial estimates (which assumed a constant speed). These solutions are not implausible. A non-constant deceleration profile is suggested as one way in which the predictions for the 24 August 1998 event may be reconciled better with observations and the predictions for the 13 May 2005 event made more consistent with the investigations of others [*Reiner et al.*, 2001].

The significant correlation coefficients and typically small time and frequency offsets found are good for a first quantitative comparison between theory and observation. They are also similar to those found in the companion paper that tests the α and β extraction methods using synthetic dynamic spectra [*Hillan et al.*, 2012]. The primary difference between the observations and theory appears to be the overprediction of the radio flux, typically by a few to 10 dB but sometimes by significantly larger amounts. Sometimes there are also differences in the frequency-time morphology, especially the prediction of additional weak emission bands. These may be due to defects in the type II theory itself, solar wind model, packing of ripples on the shock, neglect of smoothing, interpolation, or turbulence in the plasma properties at the locations of active shock ripples compared with the model grid, and/or the shock's direction of propagation with respect to Earth. Whether or not overprediction of emission intensity oftens occurs with our theory and models may be determined by studying more events. Similarly, improvements and extensions to the combined theory in the future may lead to predictions that more accurately and quantitatively predict the morphology, intensifications and flux magnitude of observed type II emission. Several such extenions have been suggested. Even now, however, the theory and iterative method for extracting shock parameters offer great potential for applications in space weather prediction. Coupling this with the direction finding abilities of the STEREO spacecraft, which may also offer the ability to eliminate possible contaminations due to AKR for example, offers a very good opportunity for further detailed type II studies.

Acknowledgments. We acknowledge financial support from the Australian Research Council and an Australian Postgraduate Award.

References

Bale, S. D., M. J. Reiner, J.L. Bougeret et al. (1999), The source region of an interplanetary type II radio burst, *Geophys. Res. Lett.*, *26*, 1573.

Bougeret, J. et al. (1995), WAVES: The radio and plasma wave investigation on the Wind spacecraft, *Space Sci. Rev.*, *71*, 231.

Brueckner, G. E., et al. (1995), The Large Angle Spectroscopic Coronagraph (LASCO), *Sol. Phys.*, *162*, 357.

Cairns, I. H. (1986), The source of free energy for type II solar radio bursts, *Proc. Astron. Soc. Aust.*,*6*, 444.

Cairns, I. H. (1987), A theory for the Langmuir waves in the electron foreshock, *J. Geophys. Res.*,*92*, 2329.

Cairns, I. H. (1988), A semiquantitative theory for the 2fp radiation observed upstream from the Earth's bow shock, *J. Geophys. Res*,*92(A3)*, 2329.

Cairns, I. H. (2011), Coherent radio emissions associated with solar system shocks, In *The Sun, the Solar Wind, and the Heliosphere v.4*, ed. by M. P. Miralles and J. S. Almeida, Springer Netherlands, p. 267.

Cairns, I. H. and S. A. Knock (2006), Predictions for dynamic spectra and source regions of type II radio bursts in the homogenous corona and solar wind, In *Planetary Radio Emissions VI*, ed. by H. O. Rucker, W. S. Kurth, and G. Mann, Verlag. Ost. Akad. Wissenchaften, p. 419.

Cairns, I. H., and D. B. Melrose (1985), A theory for the 2fp radiation upstream of the earth's bow shock , *J. Geophys. Res.*,*90(A7)*, 6637.

Cairns, I. H., and P. A. Robinson (1999), Strong evidence for stochastic growth of Langmuir-like waves in Earth's foreshock, *Phys. Rev. Lett.*,*82*, 3066.

Cairns, I. H., S. A. Knock, P. A. Robinson and Z. Kuncic (2003), Type II solar radio bursts: Theory and space weather implications, *Space Sci. Rev.*,*107*, 27.

Cairns, I. H., V. V. Lobzin, A. Warmuth, P. A. Robinson and G. Mann (2009), Direct radio probing and interpretation of the Sun's plasma density profile, *Astro. Jrnl. Lett.*,*706*, 265.

Cane, H. V.(1985), The evolution of interplanetary shocks, *J. Geophys. Res.*, *90*, 191.

Cane, H. V., N. R. Sheeley Jr., and R. A. Howard (1987), Energetic interplanetary shocks, radio emission, and coronal mass ejections, *J. Geophys. Res.*, *92(A9)*, 9869.

Cane, H. V., R. G. Stone, J. Fainberg, J. L. Steinberg, and S. Hoang (1982), Type II solar radio events observed in the interplanetary medium, I, General characteristics, *Sol. Phys.*, *78*, 187.

Dulk, G. A., W. C. Erickson, R. Manning, and J.-L. Bougeret (2001), Calibration of low frequency radio telescopes using the galactic background radiation, *Astron. Astrophys.*, *385*, 294.

Filbert, P. C., and P. J. Kellogg (1979), Electrostatic noise at the plasma frequency beyond the Earth's bow shock, *J. Geophys. Res.*, *84(A4)*, 1369.

Florens, M. S. L, I. H. Cairns, S. A. Knock, and P.A. Robinson (2007), Data-driven solar wind model and prediction of type II bursts, *Geophys. Res. Lett.*, *34*, L04104.

Gopalswamy, N., A. Lara, S. Yashiro, M. L. Kaiser, and R. A. Howard (2001), Predicting the 1-AU arrival times of coronal mass ejections, *J. Geophys. Res.*, *106*, 29, 207.

Hillan, D. S., I. H. Cairns, and P. A. Robinson (2012), Type II Solar Radio Bursts 1: Modeling and extraction of shock parameters, *in press, J. Geophys. Res.*.

Hillan, D. S., I. H. Cairns, P. A. Robinson, and A. Mohamed (2010), Prediction of background levels for the Wind WAVES instrument and implications for the galactic background radiation, *J. Geophys. Res.*, *115*, A06102, doi:10.1029/2009JA014714.

Kaiser, M. L. et al. (1998), Type II radio emissions in the frequency range from 1-14 MHz associated with the April 7, 1997 solar event, *J. Geophys. Res.*, *25*, 2501.

Knock, S. A. and I. H. Cairns (2005), Type II radio emission predictions : Sources of coronal and interplanetary spectral structure, *J. Geophys. Res.*, *110*, A01101.

Knock, S. A., I. H. Cairns, and P. A. Robinson (2003b), Type II radio emission predictions: Multiple shock ripples and dynamic spectra, *J. Geophys. Res.*, *108(A10)*, 1361.

Knock, S. A., I. H. Cairns, P. A. Robinson, and Z. Kuncic (2001), Theory of type II solar radio emission from the foreshock region of an interplanetary shock, *J. Geophys. Res.*, *106*, 25041.

Knock, S. A. I. H. Cairns, P. A. Robinson, and Z. Kuncic (2003a), Theoretically predicted properties of type II radio emission from an interplanetary foreshock, *J. Geophys. Res.*, *108(A3)*, 1126.

Lengyel-Frey, D., G. Thejappa, R. J. MacDowall, R. G. Stone, and J. L. Phillips (1997), Ulysses observations of wave activity at interplanetary shocks and implications for type II radio bursts, *J. Geophys. Res.*,*102*, 2611.

Lobzin, V. V., I. H. Cairns, and P. A. Robinson (2009), Evidence for wind-like regions, acceleration of shocks in the deep corona, and relevance of 1/f dynamic spectra to coronal type II bursts, *Astro. Jrnl. Lett.*,*677*, L129.

Lobzin, V. V., I. H. Cairns, P. A. Robinson Peter A., G. Steward, and G. Patterson (2010), Automatic recognition of coronal type II radio bursts: The Automated Radio Burst Identification System method and first observations, *Astro. Jrnl. Lett.*, *710*, L58.

Melrose, D. B. (1985), *Instabilities in Space and Laboratory Plasmas*, Cambridge Univ. Press, New York.

Meyer-Vernet, N. and C. Perche (1989), Tool kit for antennae and thermal noise near the plasma frequency, *J. Geophys. Res.*, *94*, 2405.

Michalek, G., N. Gopalswamy, and S. Yashiro (2009), Expansion Speed of Coronal Mass Ejections, *Sol. Phys.*, *260*, 401.

Nelder, J. A., and R. Mead (1965), A simplex method for function minimization, *Computer Journal,.*, *7*, 308.

Nelson, G. J., and D. B. Melrose (1985), Type II bursts, in *Solar Radiophysics*, ed. by D.J. McLean and N.R. Labrum, p. 333, Cambridge, New York.

Neugebauer, M., and J. Giacolone (2005), Multispacecraft observations of interplanetary shocks: Nonplanarity and energetic particles, *J. Geophys. Res.*,*110*, A12106.

Opitz, A. et al. (2009), Temporal evolution of the solar wind bulk velocity at solar minimum by correlating the STEREO A and B PLASTIC measurements, *Sol. Phys.*, *256*, 365.

Press, W. H., S. A. Teukolsky, W. T. Vetterling, and B. P. Flannery (1992), Numerical recipes in FORTRAN. The art of scientific computing, ed. by W. H. Press, S. A. Teukolsky, W. T. Vetterling, and B. P. Flannery, Cambridge University Press, 2nd ed.

Reiner, M. J., M. L. Kaiser, and J.-L. Bougeret (2001), Coronal and interplanetary propagation of CME/shocks from radio, in situ and white-light observations , *Astrophys. J.*, *663*, 1369.

Reiner, M. J., M. L. Kaiser, J. Fainberg, and R. G. Stone (1998), A new method for studying remote type II radio emissions from coronal mass ejection-driven shocks, *J. Geophys. Res.*, *103*, 29, 651.

Robinson, P. A.(1992), Clumpy Langmuir waves in type III radio sources *Sol. Phys.*, *139*,147.

Robinson, P. A., I. H. Cairns, and D. A. Gurnett (1993), Clumpy Langmuir waves in type III radio sources - Comparison of stochastic-growth theory with observations, *Astrophys. J.*, *407*,790.

Schmidt, J. M., and N. Gopalswamy (2008), Synthetic radio maps of CME-driven shocks below 4 solar radii heliocentric distance, *J. Geophys. Res.*, *113(A12)*, 8104.

Schulte in den Baumen, H., I. H. Cairns, and P. A. Robinson (2012), Nonzero azimuthal magnetic fields at the solar source surface: Extraction, model, and implications, *Geophys. Res. Lett.,* , *38*, L24101

Schwenn, R.,A. Dal Lago, E. Huttunen, and W. D. Gonzalez (2005), The association of coronal mass ejections with their effects near the Earth, *Ann. Geophys.*, *23*, 1033.

Wild, J. P. (1950a), Observations of the spectrum of high-intensity solar radiation at metre wavelengths. II - Outbursts, *Aust. J. Sci. Res.*, *A3*, 399.

Wild, J. P. (1950b), Observations of the spectrum of high-intensity solar radiation at metre wavelengths. III - Isolated bursts, *Aust. J. Sci. Res.*, *A3*, 541.

Wild, J.P., S. F. Smerd and A.A. Weiss (1963), Solar bursts, Annu. Rev, *Astron. Astrophys.*, *1*, 291.

Yashiro, S., et al. (2004), A catalog of white light coronal mass ejections observed by the SOHO spacecraft, *J. Geophys. Res.*, *109*, A07105.

Yuan, X., I. H. Cairns, and P. A. Robinson (2007), Simulation of electron bursts upstream of reforming shocks, *Astrophys. J.*, *671*, 439.

Zarka, P, B. Cecconi, and W.S. Kurth (2004), Jupiter's low-frequency radio spectrum from Cassini/Radio and Plasma Wave Science (RPWS) absolute flux density measurements, *J. Geophys. Res.*, *109*, A09S15.

Figure 1. Initial LASCO/SOHO C2 coronograph observations of a CME on 3 December 2004 progressing in time from left to right and top to bottom (LASCO/SOHO CME catalog *http://vso.nascom.nasa.gov/cgi-bin/vso/catalog.pl*). CME lift off occurs at 00:26 UT (top right) and develops into a "halo-like" CME, moving out in all directions.

Figure 2. Type II events observed by Wind/WAVES, displayed in dB as dynamic spectra $DB_O(t, f)$ of the measured total intensity relative to the radio background. (Top left) 3 December 2004 event starting at 00:26 UT with shock arriving 3126 min later. (Top right) 13 May 2005 event starting at 17:12 UT with shock arriving 1976 min later. (Bottom left) 13 May 2005 event with intense emission between 50-200 kHz set to 0 dB from 1200 min onward. (Bottom right) 24 August 1998 event starting at 22:09 UT with shock arriving 1950 min later.

Figure 3. Dynamic spectra $DB_T(t, f)$ predicted in dB for the initial shock evolution model (see text for parameters) and a solar wind model driven by spacecraft data for the previous solar rotation. The fundamental (F) and harmonic (H) radio emission is labeled. (Top left) 3 December 2004 event. (Top right) 13 May 2005 event. (Bottom left) 24 August 1998 event.

Figure 4. Data-driven solar wind model for solar period 16 April to 13 May 2005, calculated using the technique of *Florens et al.* [2007] and Wind spacecraft data. B_r is the radial magnetic field component with inwards and outwards sense, and θ is the angle between B and the radial direction.

Figure 5. Data-driven solar wind model for solar period 30 July to 26 August 1998, calculated using the technique of *Florens et al.* [2007] and Wind spacecraft data. B_r is the radial magnetic field component with inwards and outwards sense, and θ is the angle between B and the radial direction.

Figure 6. The following dynamic spectra are plotted on the same dB scale for comparison. (Top left) Observed type II on 3 December 2004. (Top right) Shock evolution for the simulated 3 December 2004 event, plotted at times $t = 500$ min, $t = 1500$ min, and $t = 3000$ min from left to right. The initial shock model is plotted in blue, the α solution in red, and the β solution in green (see text for parameters). (Bottom left) Simulated dynamic spectrum for the shock model extracted using the α parameter. (Bottom right) Simulated dynamic spectrum for the shock model extracted using the β parameter.

Figure 7. The following dynamic spectra are plotted on the same dB scale for comparison. (Top left) Observed type II on 13 May 2005. (Top right) Shock evolution for the simulated 13 May 2005 event, plotted at times $t = 250$ min, $t = 1000$ min, and $t = 1976$ min from left to right. The initial shock model is plotted in blue, the α solution in red, and the β solution in green (see text for parameters). (Bottom left) Simulated dynamic spectrum for the shock model extracted using the α parameter. (Bottom right) Simulated dynamic spectrum for the shock model extracted using the β parameter.

Figure 8. The following dynamic spectra are plotted on the same dB scale for comparison. (Top left) Observed type II on 24 August 1998. (Top right) Shock evolution for the simulated 24 August 1998 event, plotted at times $t = 250$ min, $t = 1000$ min, and $t = 1950$ min from left to right. The initial shock model is plotted in blue, the α solution in red, and the β solution in green (see text for parameters). (Bottom left) Simulated dynamic spectrum for the shock model extracted using the α parameter. (Bottom right) Simulated dynamic spectrum for the shock model extracted using the β parameter.

Figure 9. Plots of the mean and peak fluxes in dB as a function of frequency for each of the events studied. From the top row to the bottom row, the 3 December 2004 event, the 13 May 2005 event, and the 24 August 1998 event. In each subplot the solid black line shows the observed data, the blue dots show the prediction for the initial shock model, and the red crosses and green squares show the predictions for the α and β solutions, respectively. In the case of the 13 May 2005 event, the dashed black line shows the observed data with the possible source of AKR removed. Note that outside of the displayed frequency range the predicted fluxes essentially drop away to zero.

Table 1. Amoeba starting simplex parameter ranges for extracting shock parameters for the three type II events studied. The columns list the minimum and maximum ranges for the randomly chosen parameters at each vertex.

Parameter	Minimum	Maximum
v_i (km s^{-1})	1200	1900
s	0.1	2.0
d	0.00	1.00

Table 2. Summary of results using initial shock parameters from LASCO/SOHO (L/S) estimates and the shock parameters extracted using the two Amoeba fitting methods. Each row lists, from left to right, how the parameters were obtained, the parameters extracted, and the values of each assessment parameter.

Method	Parameters				Results			
	v_i	a	s	d	$C_{\max}$	(t_0, f_0)	α	β
3 December 2004								
L/S	1350	−5.8	1.0	0.0	0.24	(77,5)	2.63×10^{-2}	2.88×10^{5}
α	1425 ± 1	−6.7	1.1 ± 0.01	0.42 ± 0.01	0.24	(1,5)	9.10×10^{-3}	2.86×10^{5}
β	1490 ± 6	−7.4	0.6 ± 0.1	0.35 ± 0.02	0.18	(36,8)	1.86×10^{-2}	2.76×10^{5}
13 May 2005 event								
L/S	1690	−7.2	1.0	0.0	0.32	(64,23)	5.29×10^{-2}	1.64×10^{5}
α	1515 ± 5	−4.3	2.9 ± 0.1	0.37 ± 0.01	0.33	(0,20)	3.64×10^{-2}	1.59×10^{5}
β	1385 ± 2	−2.1	3.0 ± 0.1	0.15 ± 0.02	0.35	(5,21)	3.83×10^{-2}	1.56×10^{5}
24 August 1998								
L/S	1300	−0.4	1.0	0.37	0.33	(193,0)	9.90×10^{-2}	2.14×10^{5}
α	1980 ± 4	−12.0	2.3 ± 0.1	0.83 ± 0.01	0.39	(0,2)	3.64×10^{-2}	2.11×10^{5}
β	1592 ± 1	−5.4	3.4 ± 0.2	0.25 ± 0.01	0.39	(136,6)	7.06×10^{-2}	2.10×10^{5}

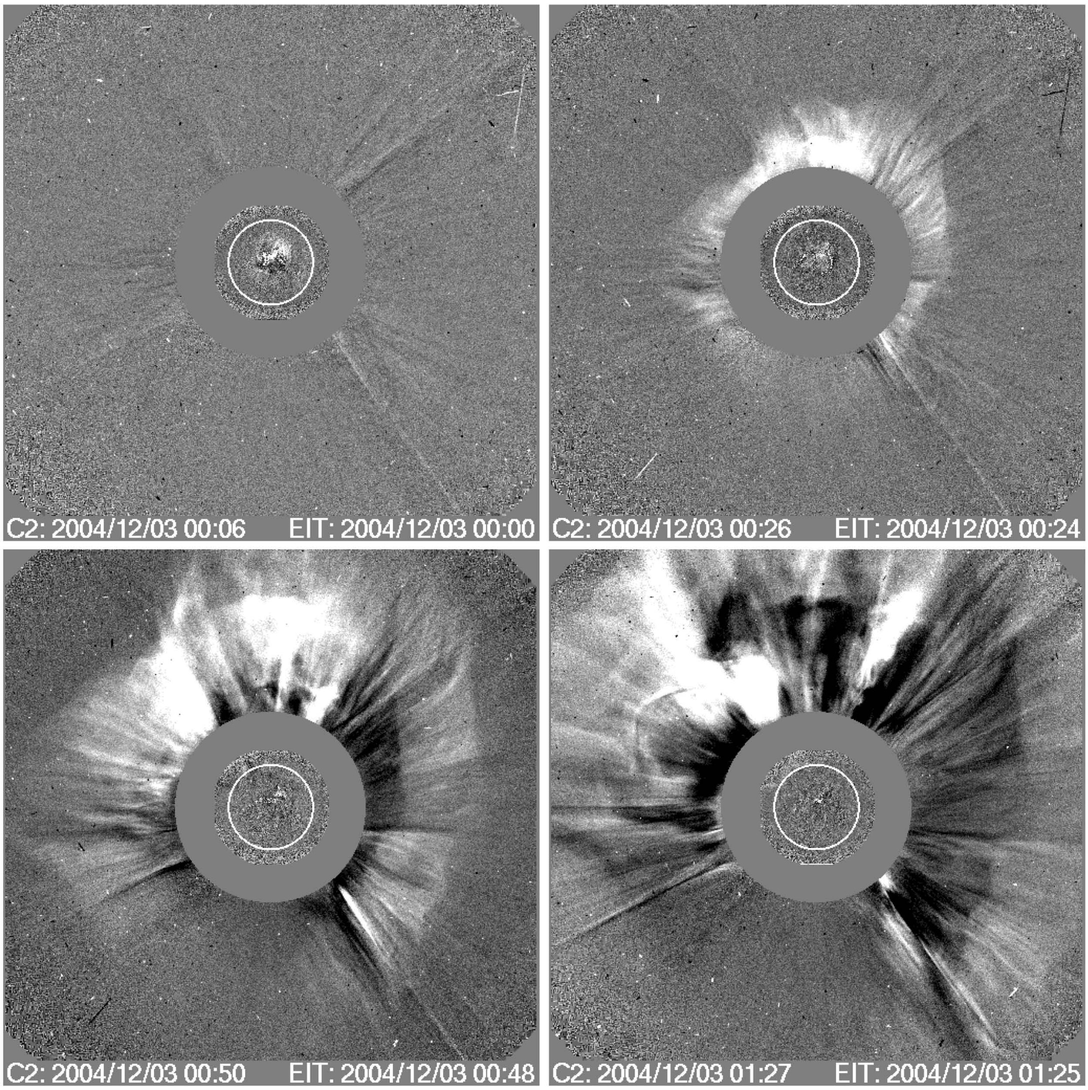
C2: 2004/12/03 00:06
EIT: 2004/12/03 00:00
C2: 2004/12/03 00:26
EIT: 2004/12/03 00:24
C2: 2004/12/03 00:50
EIT: 2004/12/03 00:48
C2: 2004/12/03 01:27
EIT: 2004/12/03 01:25

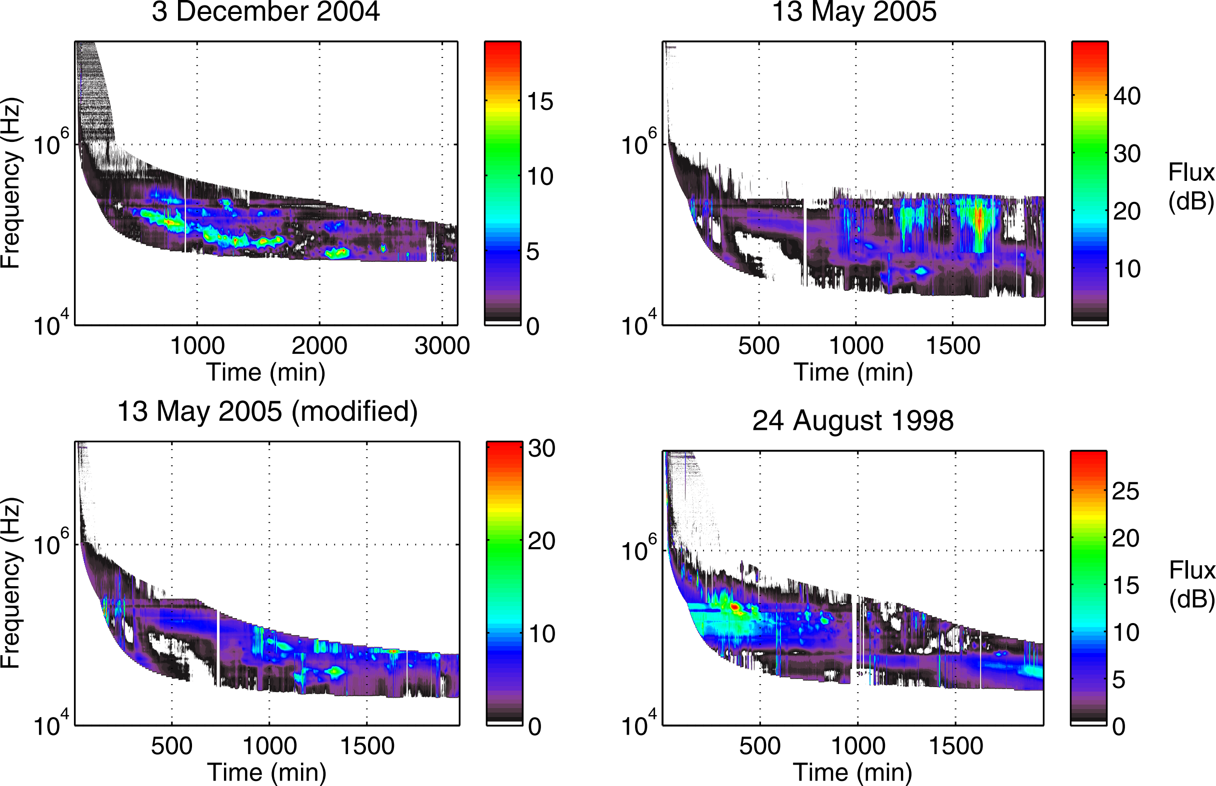

3 December 2004
13 May 2005
13 May 2005 (modified)
24 August 1998
Frequency (Hz)
10^6
10^4
Time (min)
1000
2000
3000
500
1500
Flux (dB)
0
5
10
15
20
25
30
40

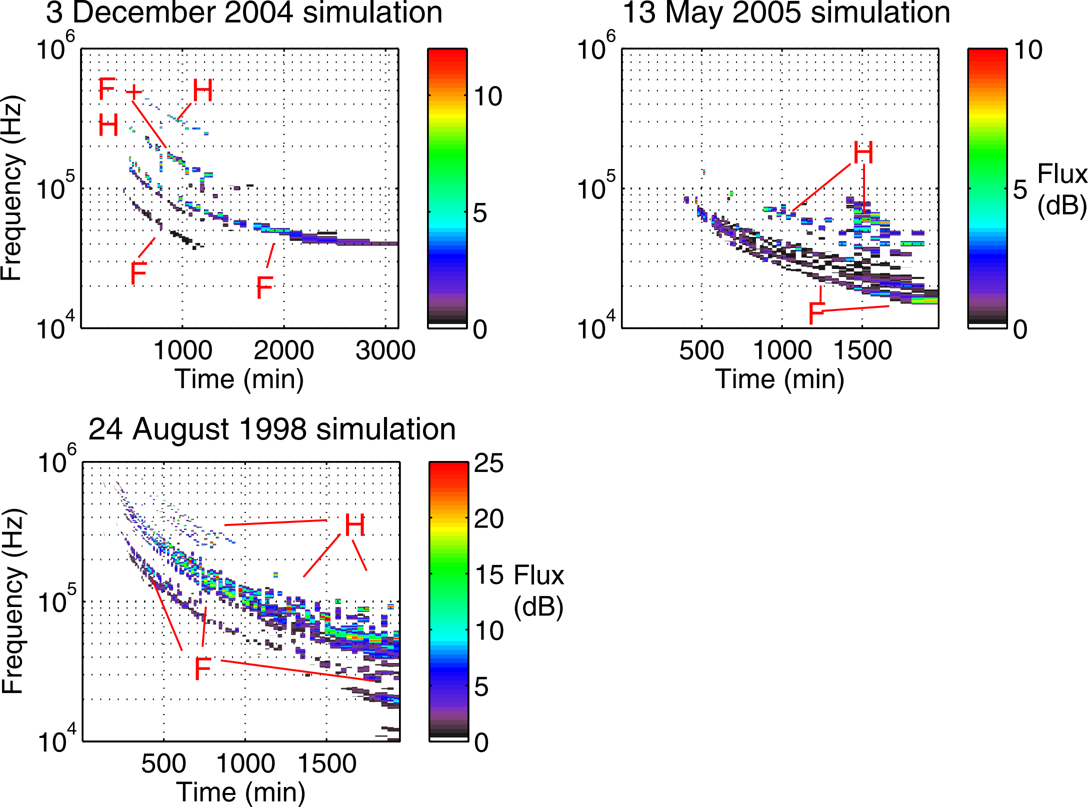

3 December 2004 simulation
13 May 2005 simulation
24 August 1998 simulation
Frequency (Hz)
Time (min)
F + H
H
F
Flux (dB)

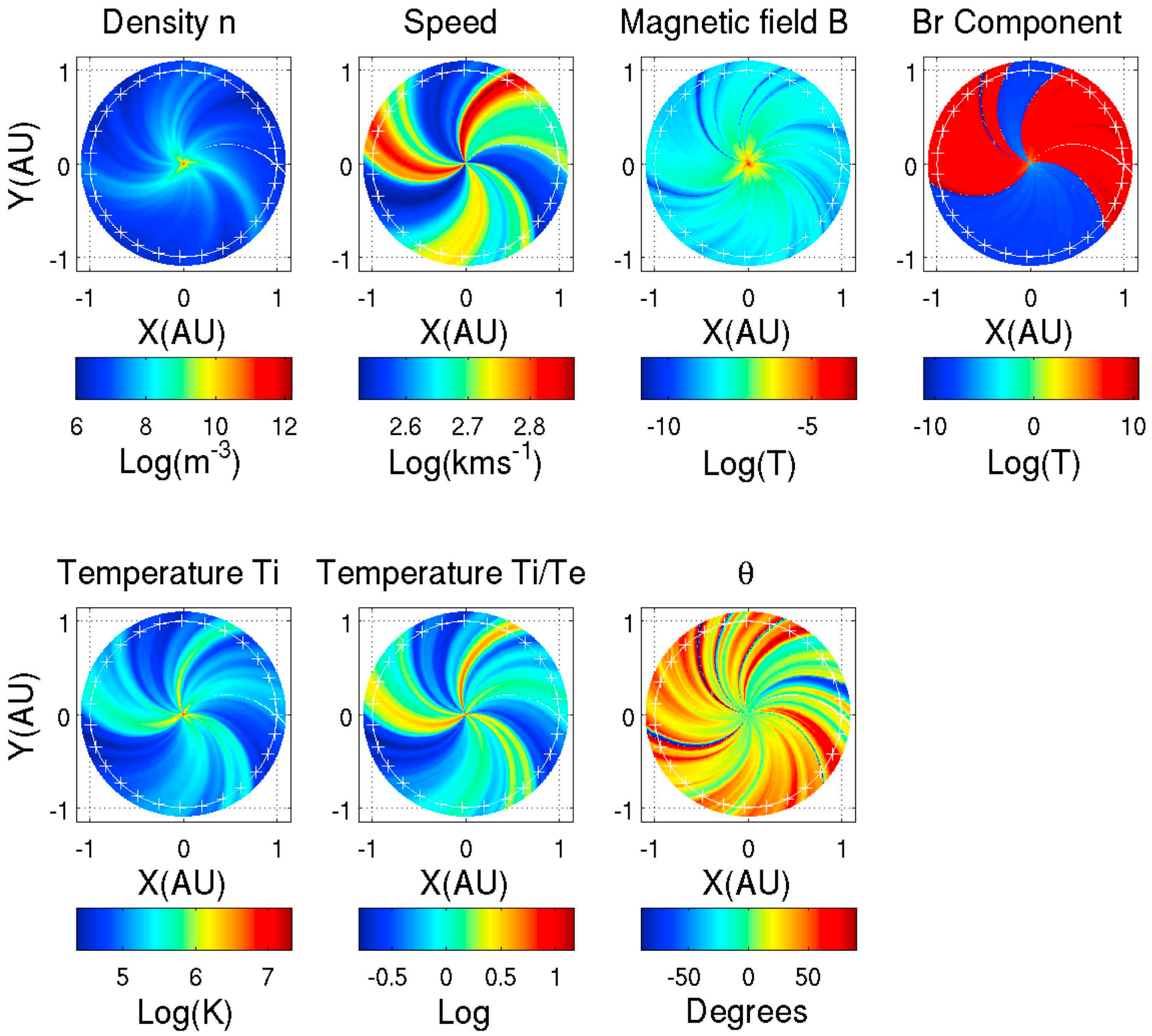

Density n
Speed
Magnetic field B
Br Component
Y(AU)
X(AU)
Log(m^-3)
Log(kms^-1)
Log(T)
Log(T)
Temperature Ti
Temperature Ti/Te
θ
Log(K)
Log
Degrees

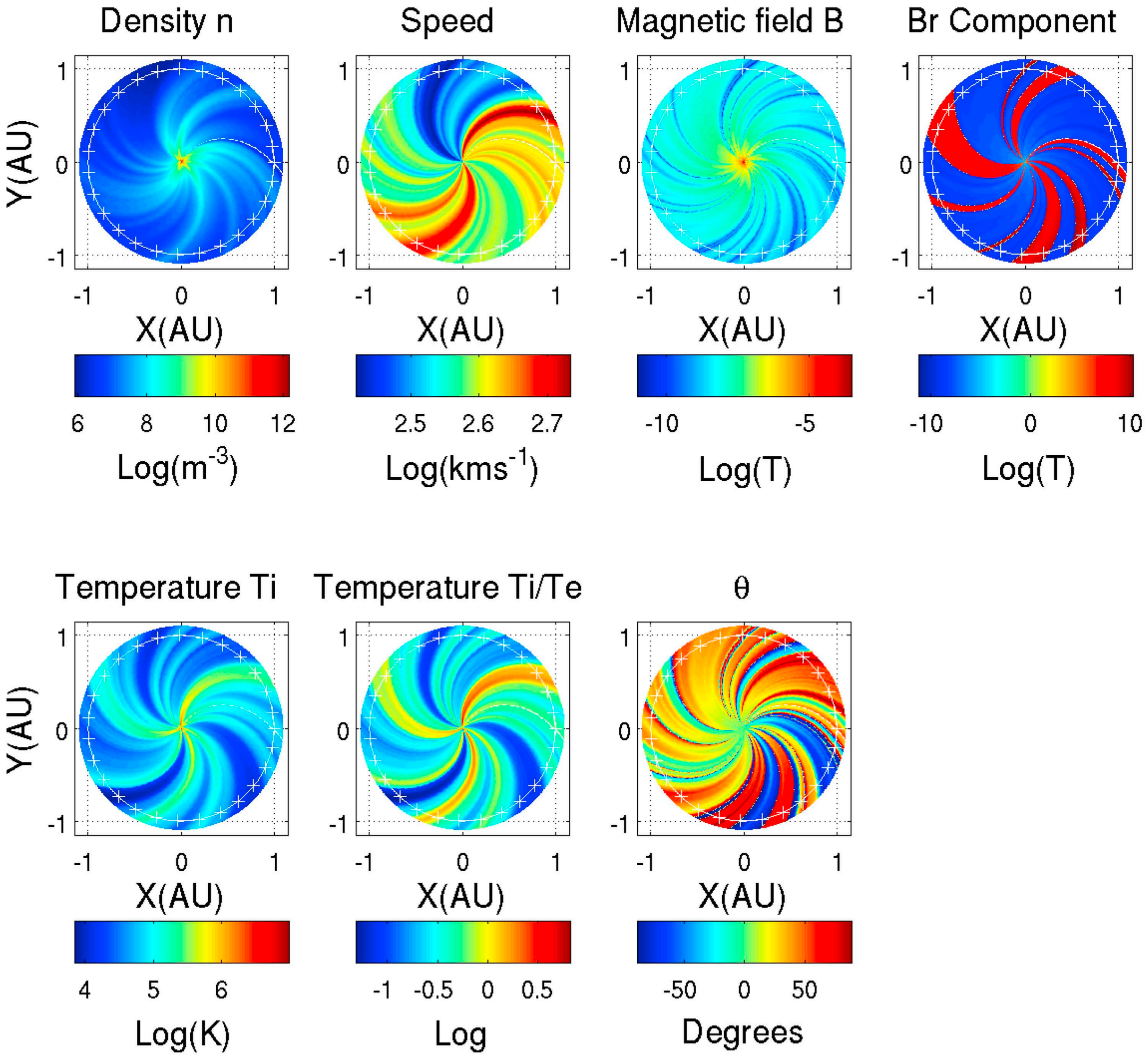

Density n
Speed
Magnetic field B
Br Component
Y(AU)
X(AU)
Log(m^-3)
Log(kms^-1)
Log(T)
Log(T)
Temperature Ti
Temperature Ti/Te
θ
Log(K)
Log
Degrees

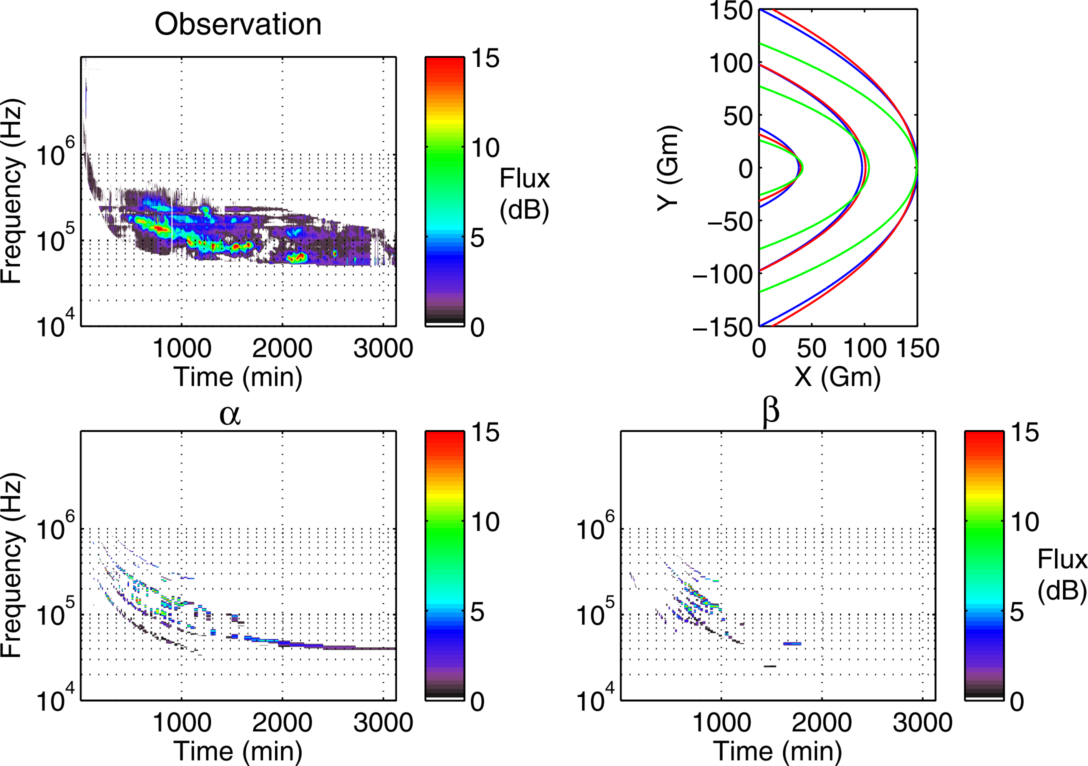

Observation
Frequency (Hz)
Time (min)
Flux
(dB)
Y (Gm)
X (Gm)
α
β

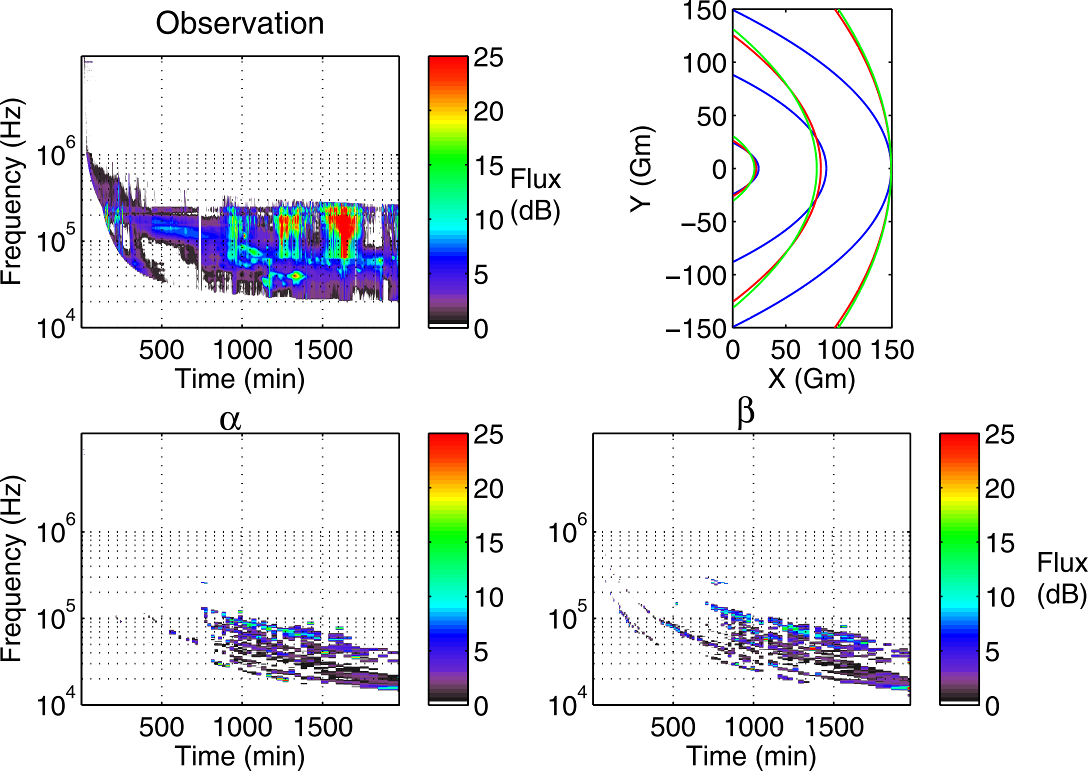

Observation
Frequency (Hz)
Time (min)
Flux (dB)
Y (Gm)
X (Gm)
α
β
Frequency (Hz)
Time (min)
Time (min)
Flux (dB)

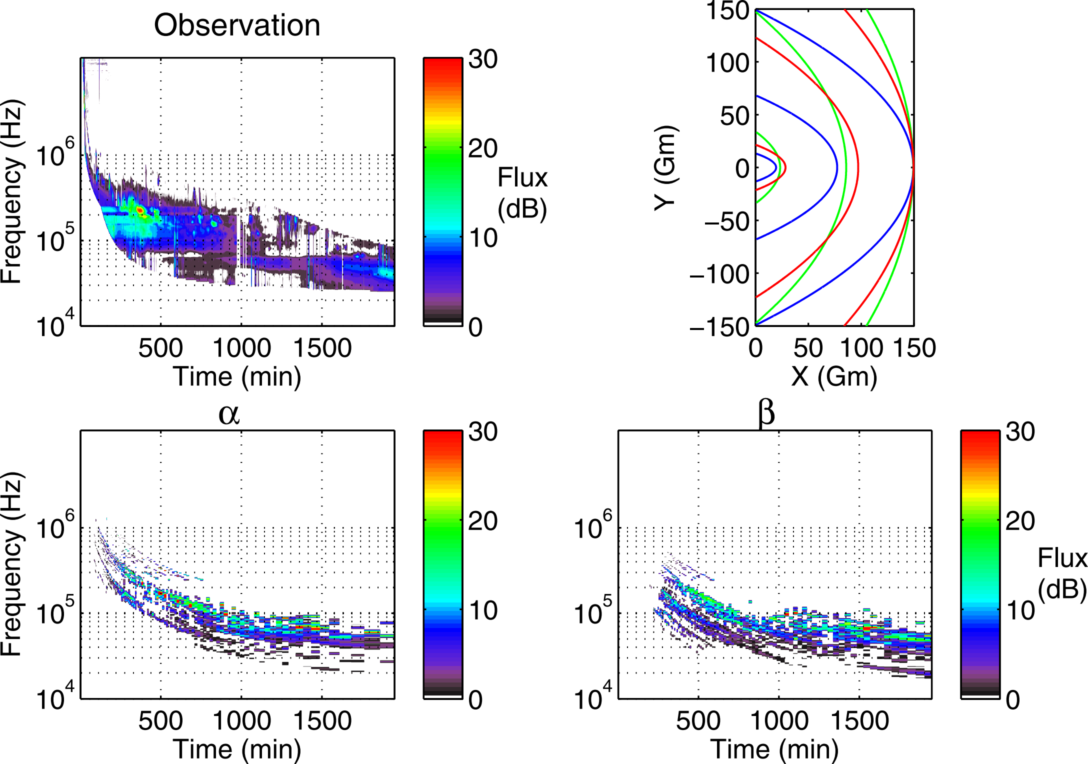
Observation
Frequency (Hz)
Time (min)
Flux (dB)
Y (Gm)
X (Gm)
α
β

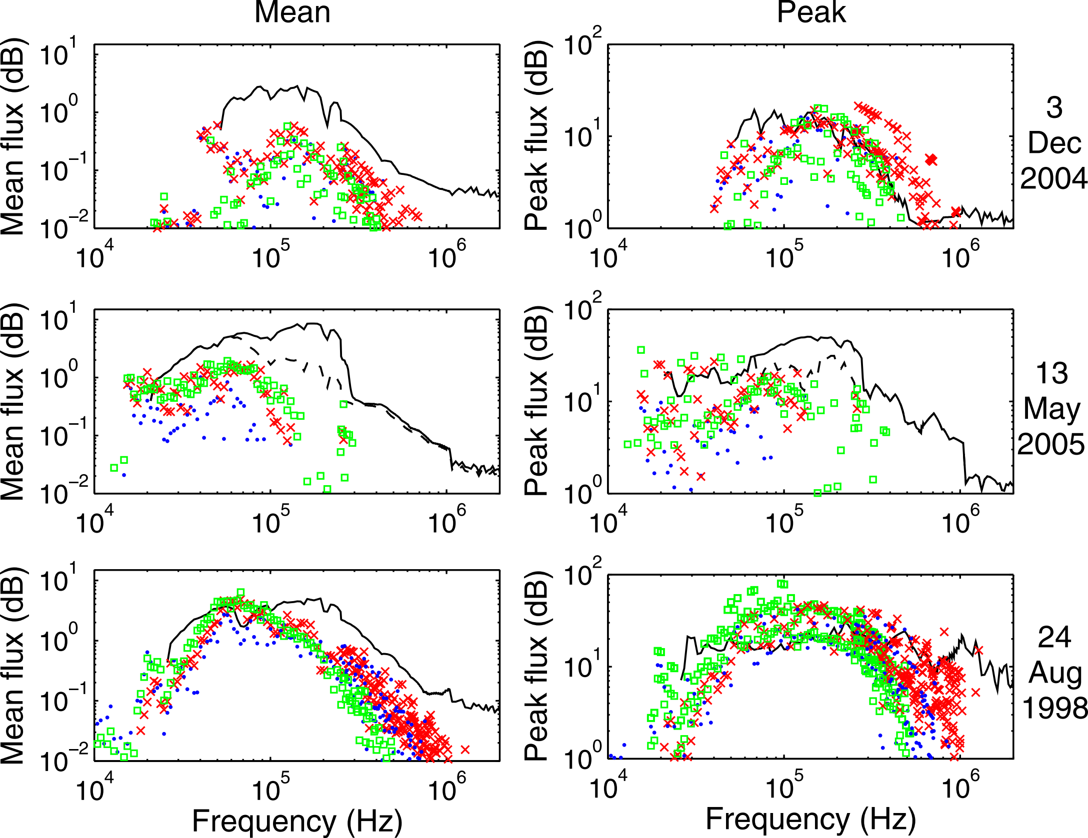

Mean
Peak
Mean flux (dB)
Peak flux (dB)
Frequency (Hz)
3 Dec 2004
13 May 2005
24 Aug 1998